A&A 464, 609–614 (2007)
DOI: 10.1051/0004-6361:20065801
© ESO 2007

Astronomy & Astrophysics

The Galactic distribution of magnetic fields in molecular clouds and HII regions⋆

J. L. Han[1] and J. S. Zhang[2,3]

[1] National Astronomical Observatories, Chinese Academy of Sciences, Jia-20 DaTun Road, ChaoYang District, Beijing 100012, PR China
e-mail: hjl@bao.ac.cn
[2] Center for Astrophysics, Guangzhou University, Guangzhou 510400, PR China
[3] Purple Mountain Observatory, Chinese Academy of Sciences, Nanjing 210008, PR China

Received 11 June 2006 / Accepted 27 October 2006

ABSTRACT

Aims. Magnetic fields exist on all scales in our Galaxy. There is a controversy about whether the magnetic fields in molecular clouds are preserved from the permeated magnetic fields in the interstellar medium (ISM) during cloud formation. We investigate this controversy using available data in the light of the newly revealed magnetic field structure of the Galactic disk obtained from pulsar rotation measures (RMs).

Methods. We collected measurements of the magnetic fields in molecular clouds, including Zeeman splitting data of OH masers in clouds and OH or HI absorption or emission lines of clouds themselves.

Results. The Zeeman data show structures in the sign distribution of the line-of-sight component of the magnetic field. Compared to the large-scale Galactic magnetic fields derived from pulsar RMs, the sign distribution of the Zeeman data shows similar large-scale field reversals. Previous such examinations were flawed in the over-simplified global model used for the large-scale magnetic fields in the Galactic disk.

Conclusions. We conclude that the magnetic fields in the clouds may still "remember" the directions of magnetic fields in the Galactic ISM to some extent, and could be used as complementary tracers of the large-scale magnetic structure. More Zeeman data of OH masers in widely distributed clouds are required.

Key words. ISM: molecules – ISM: magnetic fields – masers – magnetic fields – Galaxy: structure

1. Introduction

The interstellar space is filled with HI gas, with a density of n_e of about 1 cm^{-3}. The interstellar medium is not uniformly distributed; rather, it is clumped. In some regions, the density is very high and partially ionized, appearing as clouds with a size of several pc and a density of $n_e \sim 10^2$ to 10^3 cm^{-3}. There are cores in some clouds, where the density can be as high as 10^7 cm^{-3} and stars can be formed there.

Magnetic fields permeate the interstellar medium as well as the clouds. In some clouds, magnetic fields are the dominant force against collapse by self-gravity. Such clouds have been observed to have an hourglass morphology, which indicates the strong regular magnetic field near the core (see review of Heiles & Crutcher 2005). The strength of magnetic fields in clouds $|B|$ scales with the density ρ as $|B| \propto \rho^{\sim 0.5}$ (Crutcher 1999). The magnetic fields in clouds may be preserved when the clouds were formed by contraction of diffuse interstellar medium. The question then rises as to: whether or not the magnetic fields in molecular clouds can still "remember" the large-scale magnetic fields in the interstellar medium. Are they sufficiently strong that their correlation with the large-scale fields was not destroyed by turbulence in clouds? If so, the clouds can be an independent approach to reveal the large-scale structure of Galactic magnetic fields. Conclusions from previous researches on this subject (Davies 1974; Reid & Silverstein 1990; Baudry et al. 1997; Fish et al. 2003a) are contradictory.

Magnetic fields in molecular clouds have been detected through observations of Zeeman splitting of spectral lines for the line-of-sight strength, and through polarized thermal emission from dust at mm, sub-mm or infrared wavelengths for the transverse orientation of the fields. It is difficult to observe the magnetic fields in diffuse interstellar medium and molecular clouds (Heiles & Crutcher 2005), because of the weakness of fields and difficulties of calibration. Masers in massive star formation regions near high density cloud cores, with a scale size of 100 AU, are very bright (often >1 Jy) and their Zeeman splitting is relatively easier to measure since the magnetic fields in such a dense region are very strong, typically a few milligauss (mG).

From Zeeman splitting data of a small sample of eight OH masers in the ultra-compact HII regions excited by the central OB stars as well as of seven HI clouds, Davies (1974) first noticed that the line-of-sight direction of magnetic fields in all these clouds is parallel to the direction of Galactic rotation, i.e. clockwise when viewed from the north Galactic pole. Reid & Silverstein (1990) pursued the idea and examined published data available at that time, and obtained a sample of 17 reliable OH maser sources with detectable Zeeman pairs. They noticed that 14 of 17 sources have line-of-sight magnetic field directions coincident with the direction of the Galactic rotation, confirming the result of Davies (1974). This surprising result is consistent with the magnetic fields in the local arm region determined

⋆ Tables 1 and 2 are only available in electronic form at http://www.aanda.org

Article published by EDP Sciences and available at http://www.aanda.org or http://dx.doi.org/10.1051/0004-6361:20065801

by pulsar RMs at that time (Manchester 1974). The implication is that the magnetic fields in the molecular clouds are preserved during contraction from interstellar medium to star formation region in clouds. Caswell & Vaile (1995) observed 17 clouds with magnetic fields in the the direction of Galactic rotation but also 11 in the counter-rotation direction. Baudry et al. (1997) used their observations of 14 OH sources, together with 32 from the literature, and showed that 28 of 46 sources have fields in the direction of Galactic rotation (clockwise) and the other 17 sources in the counterclockwise direction, excluding one near the Galactic center. Fish et al. (2003a) identified 45 sources from survey observations of massive star-formation regions, plus 29 sources in the literature. They found that 41 of 74 sources are consistent with magnetic fields in a clockwise sense, and 33 with fields in a counterclockwise sense. This gives the impression that the maser data cannot be used to reveal the global field structure of our Galaxy.

The large-scale magnetic structure in the Galactic disk does not have one dominant sense as originally hypothesized by Davies (1974). It has many reversals. Recently Han et al. (2006) measured a large sample of pulsar RMs and presented clear evidence for large-scale counterclockwise fields in the spiral arms interior to the Sun and weaker evidence for a counterclockwise field in the Perseus arm. In interarm regions, including the Solar neighborhood, the evidence suggests that large-scale fields are clockwise.

In this paper we collect all measurements of magnetic fields in star formation regions as well as in molecular clouds, and compare them with the magnetic field configuration newly derived from pulsar RM data. The kinematic distances of molecular clouds or star formations regions are unified to the frame of $R_0 = 8.5$ kpc and $V_\odot = 220$ km s^{-1}. All magnetic field measurements from Zeeman splitting observations are for the line-of-sight component.

2. Collected Zeeman splitting data for cloud magnetic fields

Two methods have been used to measure the magnetic fields of molecular clouds. The classical one is to observe the Zeeman splitting of HI or OH lines (see below), which gives the strength of the magnetic field along the line of sight. The second one is to map the polarization of clouds at mm, submm or infrared (e.g. Chuss et al. 2003), which can show the magnetic field orientation in the sky-plane. However, there are not many molecular clouds mapped by polarization. Therefore we will only collect the Zeeman splitting data.

Zeeman splitting of spectral lines occurs in two kinds of regions. OH or other emission lines are very strong from maser spots in high density HII regions or star formation regions, mainly in the ionized surrounding of newly formed stars in molecular clouds. There is much data for this kind of observation. The emission or absorption lines (OH or HI) are also observed for nearer layers of clouds. We surveyed the literature for both types of observations.

2.1. Zeeman splitting observations of masers

In the core of molecular clouds (often a star-formation region or HII region), maser spots have been observed in the shock-front or ionization-front surrounding newly formed stars (e.g. Reid et al. 1980; Zheng et al. 2000). We collected all measurements of Zeeman splitting of OH masers ($10^5 \sim 10^8$ cm^{-3}), but not H_2O masers for higher density regions ($\sim 10^{10}$ cm^{-3}). These data give the line-of-sight direction of magnetic fields in situ at the location of masers. One cloud often has many maser spots, and they show different field strengths and sometimes different field directions, but always indicating an organized magnetic field structure (e.g. Fish et al. 2005a; Fish & Reid 2006; Bartkiewicz et al. 2005).

Masers have been observed with different resolutions using single-dish telescopes (e.g. Parkes, Effelsberg) or interferometers (e.g. VLA or ATCA, EVN or VLBA). It is important to have high resolution observations to identify maser spots and derive the magnetic fields in each of them. On the other hand, estimates for the magnetic fields from single dish observations of masers can still be useful and meaningful if there is no confusion (simple patterns) in the spectra of masers. Although a low-resolution telescope beam would significantly reduce the Zeeman splitting, being the intensity-weighted average even if all masers have the same sign but are displaced in velocity (see Sarma et al. 2001), the inferred field strength can be the mean value of the magnetic fields at all maser spots (e.g. Caswell 2004a).

In Table 1, we list OH maser measurements collected from the literature. We discarded the measurements with grade "D" in Fish et al. (2003a) which are thought not to be reliable identifications as the authors have claimed; and we also take the middle value if a field strength range is given in their data. We give the two extremes as well as the median value for magnetic field measurements in the table. If there is only one measurement for a cloud, such as from the Parkes telescope by Caswell (see references in the Table 1), or only for one maser spot from VLBI observations, we give them in the median value. We sometimes discard old measurements if there are too many new high resolution observations available. Care should be taken to avoid misinterpretation of the data, such as G285.26−0.05 at 1665 MHz in Davies (1974), see discussions in Caswell & Vaile (1995). The signs for field directions were sometimes not given in the data tables (e.g. Gaume & Mutel 1987; Baudry & Diamond 1998; Desmurs et al. 1998), so one has to look at the original plots of the RH/LH maser spectrum, or text, or other references to identify their signs. In some papers measurements were discussed in the text rather than expressed in data tables (e.g. Caswell & Vaile 1995). Distances of most of Caswell's table are given with the old IAU standard (10 kpc/220 km s^{-1}) and should be corrected to the current one (8.5 kpc/220 km s^{-1}). For ambiguous kinematic distances we take the nearer one but marked it with an asterisk after the value. We updated the distances of some HII regions according to the latest reference (e.g. Fish et al. 2003b). If one object has many observations (e.g. of many lines), one good measurement was selected as representative of the cloud. For this purpose we normally take the best result from high resolution spatial observation or the median of the many median values, as marked with a "*".

We did not use the Zeeman splitting data of OH masers associated with proto-planetary nebulae, supernova remnants, or young stellar objects for our study.

2.2. Zeeman splitting observations of molecular clouds

We searched the literature for measurements of magnetic fields in molecular clouds. Crutcher (1999) has collected good measurements of 15 clouds in Table 1 of his paper with detailed discussions on each cloud in the appendix. We complemented this data with new measurements, and present them in Table 2. The sources are given in the order of Galactic coordinates. The relative information, such as distance, the emission or absorption

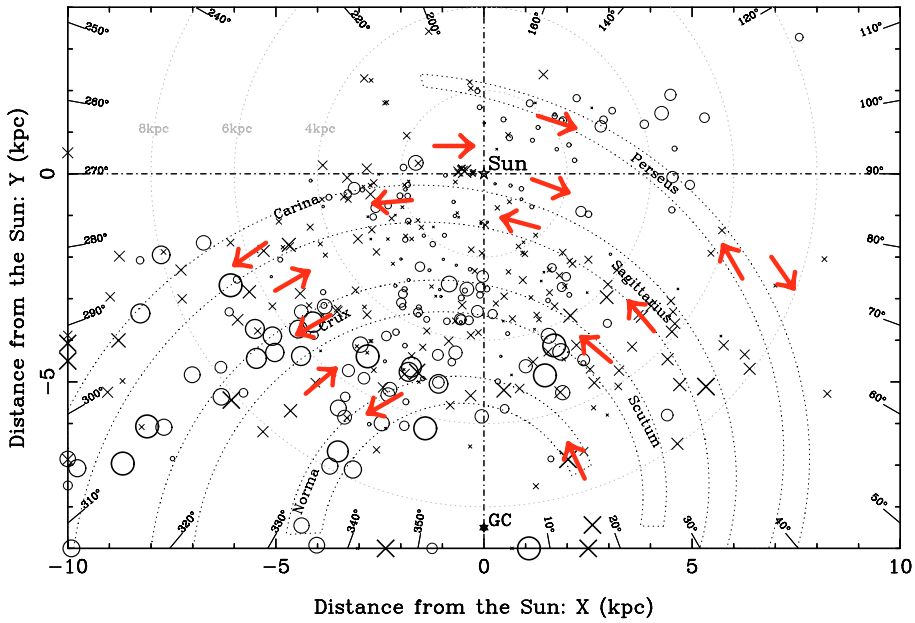

Fig. 1. The RM distribution of 374 pulsars with $|b| < 8°$, projected onto the Galactic Plane. The linear sizes of the symbols are proportional to the square root of the RM values, with limits of 9 and 900 rad m^{-2}. The crosses represent positive RMs (indicating the average field over path pointing towards us), and the open circles represent negative RMs (for the average fields going away from us). The approximate locations of four spiral arms are indicated. The large-scale structure of magnetic fields derived from pulsar RMs are indicated by thick arrows. See Han et al. (2006) for details.

line observed, the instruments as well as the frequency of observations are also given. Observations of one object but by different authors or different emission or absorption lines are listed in different lines in the table. Note that different observation resolutions can cause different results (see e.g. Brogan & Troland 2001a), so we also list the telescopes used for observations. Similarly, we take the median of the many observations or the measurement of highest quality as a representative of a cloud. For these we mark a "*" after the field strength.

We do not include the magnetic field measurements of diffuse clouds (e.g. Myers et al. 1995; Goodman & Heiles 1994) or HI filaments (Heiles 1989), which are not gravitationally bound and therefore are not molecular clouds. Similarly, we did not include data of Zeeman splitting of absorption lines from the cold neutral medium by observing extragalactic radio sources (e.g. Heiles & Troland 2004).

3. Analysis and discussion

The HII regions and molecular clouds are confined to the Galactic plane, and are regarded as tracers of the spiral arms. Here we extend the work by Fish et al. (2003a), in light of the newly derived magnetic field configuration associated with spiral arms in the Galactic disk from pulsar RMs (Han et al. 2006) as well as more measurements of magnetic fields from masers and molecular clouds.

3.1. The Galactic magnetic fields derived from pulsar RMs

The large-scale magnetic fields in the Galactic disk have been derived from pulsar RMs (Han et al. 2006). The variation of RMs with the dispersion measures of pulsars indicates the magnetic field direction (see arrows in Fig. 1). There are many reversals of large-scale magnetic fields. In some regions pulsar data were rich enough to derive the magnetic field direction. However, the fields in many other regions cannot be determined due to scarcity of data points. Also, random fields in some regions may be stronger than the regular magnetic fields, which complicates derivation of field directions from pulsar data. Our current knowledge of large-scale magnetic fields is shown in Fig. 1, very different from the over-simplified field structure used in previous studies (e.g. Davies 1974).

At high Galactic latitudes, Han et al. (1997, 1999) identified a striking antisymmetry in the RM distribution in the sky, mainly in the inner Galaxy, which was argued as being caused by azimuthal magnetic fields in the Galactic halo with reversed field directions below and above the Galactic plane. However, there is little Zeeman splitting data for the molecular clouds at high Galactic latitudes (see Tables 1 and 2 below), so we will not discuss these data for the halo field. Instead, we concentrate on the large-scale field in the Galactic disk.

3.2. Overview of the data

We plot the measurements of Zeeman splitting for magnetic fields in Fig. 2, using the median values in Tables 1 and 2. The medians are good representatives if many spots are observed with high resolution observations for the Zeeman splitting in molecular clouds or star formation regions (e.g. Fish & Reid 2006; Fish et al. 2005b). If there are measurements for only two spots, then we took their average. Given the fact that the large-scale magnetic fields in the Galactic disk are not in one field sense (clockwise) as assumed in many previous analyses, it is not meaningful to count how many data points have the same sense as the Galactic rotation and how many have the opposite sense. Rather, we should compare data with proposed models for the magnetic fields in the Galactic disk.

As seen in Fig. 2, the sign distribution of Zeeman splitting data have a clear structure. In many regions there is a dominant direction of line-of-sight components, which can be related to the clockwise (CW) or counterclockwise (CCW) sense of the Galactic azimuthal magnetic fields. As discussed by

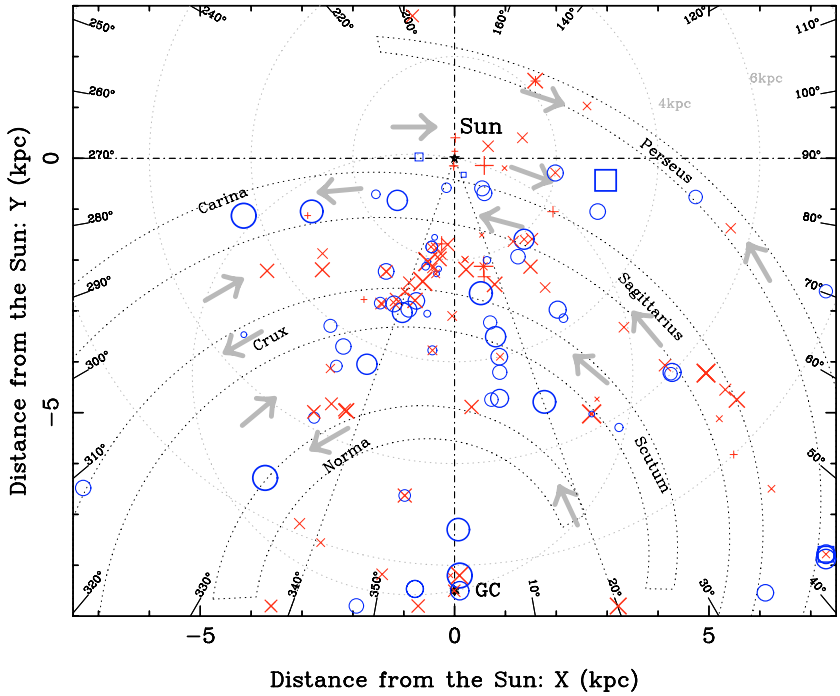

Fig. 2. The medians of field measurements from Zeeman splitting of OH masers (cross and circles) in 137 objects or HI or OH lines of 17 molecular clouds (plus and squares) projected onto the Galactic plane, with the rough indication of spiral arms and the magnetic field directions (arrows) derived from pulsar RM data. The linear sizes of the symbols are proportional to the square root of the field-strength values, with limits of 0.5 and 9 mG for fields from the median maser fields and of 15 μG and 270 μG for median cloud fields. The crosses or pluses on the right ($0^\circ < l < 180^\circ$) represent positive B, ie. the field direction going away from observer, and circles or squares going towards us. The symbols on the left ($180^\circ < l < 360^\circ$) are reversed, so that all crosses and pluses are consistent with the clockwise fields viewed from the Northern Galactic pole, and all circles and squares with counterclockwise fields.

Fish et al. (2003a), most measurements (8 crosses or pluses of 10 data) outside the solar circle are consistent with a CW large-scale field nearer than or around the Perseus arm. Second, most data points (circles) in the Carina arm are consistent with a counterclockwise (CCW) large-scale field derived from pulsar RMs. As noticed by Fish et al. (2003a), masers (crosses) in the Sagittarius arm at distances farther than 6 kpc show a coherent sense of CCW field direction that is in contrast to the large-scale field from pulsar RMs. However the location of the arm has a large uncertainty, very probably shifted inwards (see Cordes & Lazio 2002). Third, between the Carina-Sagittarius arm and the Crux-Scutum arm, Zeeman splitting data show the very dominant CW sense (crosses). Going inwards, one can see that data (more circles) are dominantly consistent with CCW large-scale fields in or near the Crux and Scutum arms. The data (crosses) near the Norma arm show a reversed CW field, consistent with the directions of the interarm field derived from pulsar RM data. If the large uncertainty of kinetic distances of molecular clouds or maser regions is considered, such field reversals are similar to those newly identified by Han et al. (2006) from pulsar RMs.

3.3. Indication for large-scale field reversals?

Fish et al. (2003a) suggested that the magnetic fields revealed by masers are ordered or correlated on a scale of a few kpc. Here we tried to check the sense-correlation of the data shown in Fig. 2. If there is no significant correlation, then the data do not contain information about large-scale fields.

We take +1 for all crosses or plus in Fig. 2, and −1 for all circles or squares. Thus, a median field of maser region with a direction consistent with CW sense is marked as +1, and that

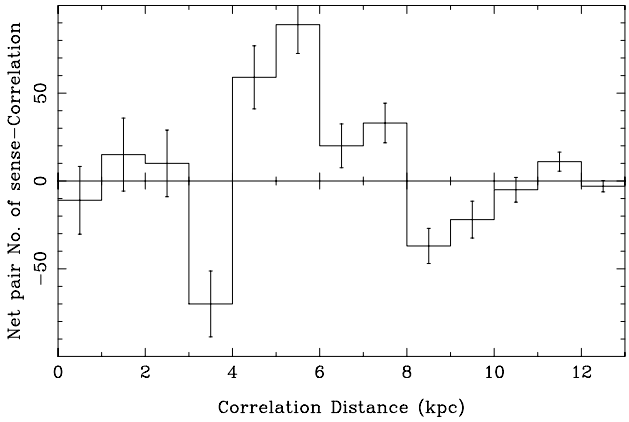

Fig. 3. Correlation for senses of magnetic field data in Fig. 2. The errorbars were estimated by $\sqrt{N}/2$, here N is the total number of pairs in a bin. See text for details.

with CCW as −1. If a pair of regions at a given distance have the same sense, they are correlated, and if they have the opposite sense, they are anti-correlated. We consider the net correlation pair numbers at different separation distances.

The results are shown in Fig. 3: pairs of objects with a separation of less than 3 kpc tend to a null correlation, due to either random fields or ordered fields along the spiral arms with opposite senses. If they are separated by 2 to 4 kpc, they tend to have the opposite sense. If they separated by 4 to 8 kpc then they tend to have the same sense. Considering the negative-positive oscillation of data probably due to sign-clusters associated with different spiral arm or interarms, though with only marginal

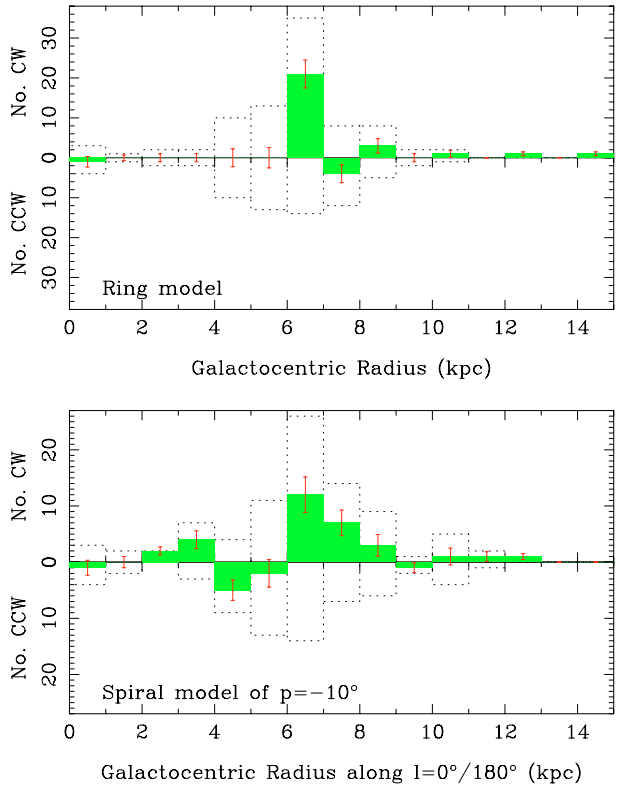

Fig. 4. The histogram of the CW and CCW senses of median magnetic fields of masers and clouds, binned for the different Galactocentric radius ranges. For the spiral model of a pitch angle of −10°, the Galactocentric radii are scaled to that along $l = 0°$ or 180°. The gray area shows the net counts in a given Galactocentric radius, and errorbars were estimated by $\sqrt{N}/2$, here N is the total number of data in a bin. Note that the field reversals have marginally been revealed by data in the frame of the spiral model.

significance, we believe that such a correlation is probably an indication of large-scale field reversals in the Galactic disk.

3.4. Models for the Galactic magnetic fields and the Zeeman splitting data

Now we can check how well the Zeeman data match the models for the large-scale magnetic fields in the Galactic disk.

There are two models for magnetic fields in the Galactic disk, a ring model in which the magnetic fields alternate their directions in many concentric rings relative to the Galactic center (Rand & Kulkarni 1989; Rand & Lyne 1994; Vallée 2005), and a spiral model in which the magnetic fields follow spiral arms but reverse their directions from arm to arm (Han & Qiao 1994; Indrani & Deshpande 1999; Han et al. 2006). We took a pitch angle of $p = -10°$ as the most probable value for the spiral.

As shown in Fig. 4, for the concentric ring model, we count how many maser regions and clouds show CW fields and how many show CCW in a given range of Galactocentric radius R_c. If the counts are roughly equal, this implies no dominant field direction in the radius range. The net counts are shown in gray, indicating the dominant field directions in those ranges. For the spiral model, assuming a pitch angle of −10°, we do the same, but the Galactocentric radius of a maser region or cloud is scaled to the Galactocentric radius R_c along $l = 0°$ or 180°.

The dominant CW field in the range of $6 < R_c < 7$ kpc is clearly shown in the ring model. The field sense is coincident with the Galactic rotation. In the ring model, there may be no large-scale fields except in this radius range. This is not true, as is shown in the magnetic fields in Fig. 1 and the sense-correlation in Fig. 2 at a distance greater than 2 or 3 kpc. The counts in the spiral model showed the field reversals from the inner Galaxy to the outer Galaxy, although some are only marginally significant, i.e., the CW fields at 2 to 4 kpc, the CCW at 4 to 6 kpc, the CW at 6 to 8 kpc and the CCW about 9 kpc and the CW field outside 9 kpc.

The dominant CW data in the Sagittarius arm are not consistent with the dominant CCW data in the Carina arm, so they diminished the net counts for the arm. The field directions given by pulsar RM data, opposite to the Zeeman data, are also similarly incompatible in the two arms. Nevertheless, all data in the two arms independently show large-scale fields in the arms.

3.5. Discussion

There are still large uncertainties in this study. One is the uncertainty in the determination of the large-scale magnetic field from pulsar RM data. Although the data have been enriched in some regions, the large-scale magnetic fields in many regions remain to be measured with more pulsar RM data (Han et al. 2006) or extragalactic radio sources (Brown et al. 2003). On the other hand, the Zeeman splitting data for *in situ* measurements of magnetic fields in clouds have two problems. One is the large uncertainty or ambiguity in the dynamic distances of clouds, which could be 10% or more (see Gómez 2006). Another problem is how to relate the field structure inside a cloud to the large-scale fields, which may be better understood after more measurements of high resolution observations become available (e.g. Fish et al. 2005a; Fish & Reid 2006). We took the median value in this study. Over many years, Caswell and Reid et al. have made detections and measurements, so that much Zeeman splitting data have been accumulated and have been included in this study. However, much more Zeeman splitting data of masers and clouds, in wider regions and high resolution observations, are needed.

Considering these uncertainties, we found that the reversals shown by data of maser regions and clouds are similar to those of large-scale magnetic fields derived from pulsar RMs. As suggested by previous authors (Reid & Silverstein 1990; Baudry et al. 1997), this may allow the use of the Zeeman splitting measurements of magnetic fields in clouds to reveal the large-scale magnetic fields in the our Galaxy.

Molecular clouds were formed by contraction of diffuse gas in the interstellar medium, and the magnetic fields are so enhanced that they have the same energy as the kinetic energy (Crutcher 1999). The role of magnetic fields during such a contraction has been observed by the hourglass shape of clouds, which is an indication of field direction conservation. Our analysis above indicates that the field direction in clouds may be preserved from the large-scale field in the ISM during the contraction.

How can such a coherence and consistence of magnetic field directions occur from the low density of ISM ($\sim$1 cm^{-3}) to higher density clouds ($\sim 10^3$ cm^{-3}), even to the highest density maser regions ($\sim 10^7$ cm^{-3}), after a density compression of about 3, or even 10, orders of magnitude? One implication of this result is that the clouds probably do not rotate much after they are formed. Otherwise, the field directions of clouds we measured would be random. During the process of star formation, the clouds seem to be too heavy to be rotated, although there are jets or disks from newly formed stars which may have some

dynamic effects. Furthermore, the fields in the molecular clouds are strong enough after the contraction so that the turbulence in the clouds cannot significantly alter the magnetic field status.

4. Conclusion

We have collected available Zeeman splitting measurements of magnetic fields in molecular clouds from the literature, and found a sign-coherency of the line-of-sight magnetic field component in many regions of the Galactic disk. Such a sign distribution is closely related to spiral arms, and shows similar field reversals to those newly derived from pulsar RM data. Thus, the magnetic fields in molecular clouds may be related to the large-scale field structure. If this can be confirmed by a larger dataset, the physical picture of the contraction of cloud formation may be better understood, in which both the density and magnetic fields are enhanced and the field directions can be preserved. The measurements of in situ magnetic fields in molecular clouds could be used as probes for the Galactic-scale magnetic field, complementary to pulsar RM data.

The molecular clouds and massive star formation regions where the masers are observed are also tracers of spiral arms. To further test whether the magnetic fields in molecular clouds are correlated with the large scale Galactic field, Zeeman splitting data from more molecular clouds are needed and their distance uncertainty or ambiguity should be resolved as well.

Acknowledgements. We thank Mr. Chen Wang for help and the anonymous referee and Prof. R. Wielebinski and Prof. E. Falgarone for helpful comments on the manuscript. J.L.H. is supported by the National Natural Science Foundation of China (10521001 and 10473015)

References

Baart, E. E., & Cohen, R. J. 1985, MNRAS, 213, 641
Baart, E. E., Cohen, R. J., Davies, R. D., et al. 1986, MNRAS, 219, 145
Bains, I., Gledhill, T. M., Yates, J. A., & Richards, A. M. S. 2003, MNRAS, 338, 287
Bains, I., Redman, M. P., Bryce, M., & Meaburn, J. 2004, MNRAS, 354, 529
Bartkiewicz, A., Szymczak, M., Cohen, R. J., & Richards, A. M. S. 2005, MNRAS, 361, 623
Baudry, A., & Diamond, P. J. 1998, A&A, 331, 697
Baudry, A., Desmurs, J. F., Wilson, T. L., & Cohen, R. J. 1997, A&A, 325, 255
Benson, J. M., Mutel, R. L., & Gaume, R. A. 1984, AJ, 89, 1391
Bourke, T. L., Myers, P. C., Robinson, G., & Hyland, A. R. 2001, ApJ, 554, 916
Brogan, C. L., Troland, T. H., Roberts, D. A., & Crutcher, R. M. 1999, ApJ, 515, 304
Brogan, C. L., Frail, D. A., Goss, W. M., & Troland, T. H. 2000, ApJ, 537, 875
Brogan, C. L., & Troland, T. H. 2001a, ApJ, 550, 799
Brogan, C. L., & Troland, T. H. 2001b, ApJ, 560, 821
Brogan, C. L., Troland, T. H., Abel, N. P., Goss, W. M., & Crutcher, R. M. 2005, ASP Conf. Ser., 343, 183
Brown, J. C., Taylor, A. R., Wielebinski, R., & Mueller 2003, ApJ, 592, L29
Caswell, J. L. 1998, MNRAS, 297, 215
Caswell, J. L. 2001, MNRAS, 326, 805
Caswell, J. L. 2003, MNRAS, 341, 551
Caswell, J. L. 2004a, MNRAS, 349, 99
Caswell, J. L. 2004b, MNRAS, 352, 101
Caswell, J. L., & Haynes, R. F. 1983a, Aust. J. Phys., 36, 361
Caswell, J. L., & Haynes, R. F. 1983b, Aust. J. Phys., 36, 417
Caswell, J. L., & Haynes, R. F. 1987, Aust. J. Phys., 40, 215
Caswell, J. L., & Reynolds, J. E. 2001, MNRAS, 325, 1346
Caswell, J. L., & Vaile, R. A. 1995, MNRAS, 273, 328
Caswell, J. L., Haynes, R. F., & Goss, W. M. 1980, Aust. J. Phys., 33, 639
Chuss, D. T., Davidson, J. E., Dotson, J. L., et al. 2003, ApJ, 599, 1116
Cordes, J. M., & Lazio, T. J. W. 2002, preprint [arXiv:astro-ph/0207156]
Crutcher, R. M. 1999, ApJ, 520, 706
Crutcher, R. M., & Kazés, I. 1983, A&A, 125, L23
Crutcher, R. M., & Troland, T. H. 2000, ApJ, 537, L139
Crutcher, R. M., Kazés, I., & Troland, T. H. 1987, A&A, 181, 119
Crutcher, R. M., Troland, T. H., Goodman, C. H., Kazes, L., & Myers, P. C. 1993, ApJ, 407, 175
Crutcher, R. M., Roberts, D. A., Mehringer, D. M., & Troland, T. H. 1996, ApJ, 462, L79
Crutcher, R. M., Roberts, D. A., Troland, T. H., & Goss, W. M. 1999a, ApJ, 515, 275
Crutcher, R. M., Troland, T. H., Lazareef, B., Paubert, G., & Kazes, I. 1999b, ApJ, 514, L121
Davies, R. D. 1974, in Galatic Radio Astronomy, IAU Symp., 60, 275
Desmurs, J. F., & Baudry, A. 1998, A&A, 340, 521
Desmurs, J. F., Baudry, A., Wilson, T. L., Cohen, R. J., & Tofani, G. 1998, A&A, 334, 1085
Edris, K. A., Fuller, G. A., Cohen, R. J., & Etoka, S. 2005, A&A, 434, 213
Fish, V. L., & Reid, M. J. 2006, ApJS, 164, 99
Fish, V. L., Reid, M. J., Agron, A. L., & Menten, K. M. 2003a, ApJ, 596, 328
Fish, V. L., Reid, M. J., Wilner, D. J., & Churchwell, E. 2003b, ApJ, 587, 701
Fish, V. L., Reid, M. J., Agron, A. L., & Zheng, X. W. 2005a, ApJS, 160, 220
Fish, V. L., Reid, M. J., & Menten, K. M. 2005b, ApJ, 623, 269
Garay, G., Reid, M. J., & Moran, J. M. 1985, ApJ, 289, 681
Gaume, R. A., & Mutel, L. M. 1987, ApJS, 65, 193
Gasiprong, N., Cohen, R. J., & Hutawarakorn, B. 2002, MNRAS, 336, 47
Gómez, G. 2006, AJ, 132, 2376
Goodman, A. A., & Heiles, C. 1994, ApJ, 424, 208
Goodman, A. A., Crutcher, R. M., Heiles, C., Myers, P. C., & Troland, T. H. 1989, ApJ, 338, L61
Han, J. L., & Qiao, G. J. 1994, A&A, 288, 759
Han, J. L., Manchester, R. N., Berkhuijsen, E. M., & Beck, R. 1997, A&A, 322, 98
Han, J. L., Manchester, R. N., & Qiao, G. J. 1999, MNRAS, 306, 371
Han, J. L., Manchester, R. N., Lyne, A. G., Qiao, G. J., & van Straten, W. 2006, ApJ, 642, 868
Hansen, S. S., Moran, J. M., Reid, M. J., Johnston, K. J., Spencer, J. H., & Walker, R. C. 1977, ApJ, 218, L65
Heiles, C. 1989, ApJ, 336, 808
Heiles, C., & Crutcher, R. 2005, in Cosmic Magnetic Fields, LNP 664, 137
Heiles, C., & Troland, T. H. 2004, ApJS, 151, 271
Hutawarakorn, B., & Cohen, R. J. 1999, MNRAS, 303, 845
Hutawarakorn, B., & Cohen, R. J. 2003, MNRAS, 345, 175
Hutawarakorn, B., & Cohen, R. J. 2005, MNRAS, 357, 338
Hutawarakorn, B., Cohen, R. J., & Brebner, G. C. 2002, MNRAS, 330, 349
Indrani, C., & Deshpande, A. A. 1999, NewA, 4, 33
Kazés, I., & Crutcher, R. M. 1986, A&A, 164, 328
Kazés, I., Troland, T. H., Crutcher, R. M., & Heiles, C. 1988, ApJ, 335, 263
Manchester, R. N. 1974, ApJ, 188, 637
Myers, P. C., Goodman, A. A., Gusten, R., & Heiles, C. 1995, ApJ, 442, 177
Niezurawska, A., Szymczak, M., Cohen, R. J., & Richards, A. M. S. 2004, MNRAS, 350, 1409
Rand, R. J., & Kulkani, S. R. 1989, ApJ, 343, 760
Rand, R. J., & Lyne, A. G. 1994, MNRAS, 268, 497
Reid, M. J., & Silverstein, E. M. 1990, ApJ, 361, 483
Reid, M. J., Haschick, A. D., Burke, B. F., et al. 1980, ApJ, 239, 89
Roberts, D. A., Crutcher, R. M., Troland, T. H., & Goss, W. M. 1993, ApJ, 412, 675
Roberts, D. A., Crutcher, R. M., & Troland, T. H. 1995, ApJ, 442, 208
Sarma, A. P., Troland, T. H., Roberts, D. A., & Crutcher, R. M. 2000, ApJ, 533, 271
Sarma, A. P., Troland, T. H., & Romney, J. D. 2001, ApJ, 554, L217
Slysh, V. I., Migenes, V., Valíts, I. E., et al. 2002, ApJ, 564, 317
Stark, D. P., Goss, W. M., Churchwell, E., Fish, V. L., & Holffman, I. M. 2006, ApJ, in press [arXiv:astro-ph/0610137]
Szymczak, M., & Gérard, E. 2004, A&A, 423, 209
Szymczak, M., Cohen, R. J., & Richards, A. M. S. 2001, A&A, 371, 1012
Troland, T. H., Crutcher, R. M., & Kazes, I. 1986, ApJ, 304, L57
Troland, T. H., Crutcher, R. M., Goodman, C. H., & Heiles, C. 1989, ApJ, 347, L89
Troland, T. H., Crutcher, R. M., Goodman, C. H., Kazes, I., & Myers, P. C. 1996, ApJ, 471, 302
Wright, M. M., Gray, M. D., & Diamond, P. J. 2004a, MNRAS, 350, 1253
Wright, M. M., Gray, M. D., & Diamond, P. J. 2004b, MNRAS, 350, 1272
Vallée, J. P. 2005, ApJ, 619, 297
van der Werf, P. P., & Goss, W. M. 1990, A&A, 238, 296
van der Werf, P. P., Goss, W. M., Heiles, C., Crutcher, R. M., & Troland, T. H. 1993, ApJ, 411, 247
Yusef-Zadeh, F., Roberts, D.A., Goss, W. M., Frail, D. A. & Green, A. J. 1999, ApJ, 512, 230
Zheng, X., Reid, M. J., & Moran, J. M. 2000, A&A, 357, L37

Online Material

Table 1. Magnetic field measurements from Zeeman splitting of OH masers.

Source (GL+GB)	Alias name	Dist (kpc)	Freq (MHz)	B_l (mG)	B_m (mG)	B_u (mG)	Obs. telescope	Ref.
G000.547−0.852	RCW 142	7.3	1667		−7.4*		VLA-A	fram03
G000.666−0.029	...	8.5	6035		−5.0*		PKS	c03
G000.666−0.034	Sgr B2M	8.2	1720		0.7		VLA-A	fram03
...	...	8.2	1720	4.5	*	10.0	VLA-C	gm87
G000.666−0.035	...	8.2	1720		9.		PKS	c04a
...	Sgr B2N	8.2	1665		1.9		VLA-C	gm87
G003.910+0.001	...	4.9	6035		5.0*		PKS	c03
G005.885−0.392	...	2.2	1720		6. *		PKS	c04a
G005.886−0.393	...	2.0	1665		1.5		VLA-A	fram03
...	...	2.0	1667	0.7		1.4	VLA-A	fram03
...	...	2.0	1665	−3.0	1.2	1.8	VLBA	fraz05
...	...	2.0	1667	−2.0	1.2*	2.0	VLBA	fraz05
...	...	2.0	1667	−2.0	0.5	1.9	VLBA	sgc+06
G008.669−0.356	...	4.8	1720		−3.		PKS	c04a
...	...	4.8	6035		−2.7*		PKS	c03
G009.622+0.195	...	5.7	1665		5.3		VLBA	fraz05
...	...	5.7	1665	−2.7		6.8	VLA-A	fram03
...	...	5.7	1667	−1.3	−0.7	6.2	VLBA	fraz05
...	...	5.7	1667		−0.1		VLA-A	fram03
G010.624−0.385	...	4.8	1667		−6.0		VLBA	fraz05
...	...	4.8	1667	−5.6	*	−3.9	VLA-A	fram03
...	OH 10.62	4.8	1667		−3.7		PKS	ch83b
G011.034+0.062	...	2.7	1720		−7.		PKS	c04a
...	...	2.7	6035		−7.7		PKS	cv95
...	...	2.7	6035		−7.7*		PKS	c03
G011.904−0.141	...	4.3*	13 441		−3.0*		PKS	c04b
G012.216−0.117	...	3.3	1665		−2.6*		VLA-A	fram03
G012.680−0.181	W33 B	4.0	1665		−4.1*		VLA-A	fram03
...	...	4.0	1667		−4.3		VLA-A	fram03
G012.908−0.259	W33 A	4.0	1667		1.4*		VLA-A	fram03
G012.908−0.260	...	3.6*	1720		−6. *		PKS	c04a
G015.034−0.677	...	2.2	6035		1.5*		PKS	c03
G017.639+0.158	...	2.6*	1720	−2.	*	14.	PKS	c04a
		2.6*	1665	−1.5			PKS	c04a
G017.639+0.155	...	2.1	1665		−0.8*		VLA-A	fram03
G019.486+0.151	...	1.6*	6035		0.3*		PKS	c03
G020.081−0.135	...	12.3	1665	6.3		9.7	VLA-A	fram03
...	G20.1−0.1	12.3	1665	6.	7. *	7.	VLA-CD	grm85
G020.237+0.065	...	5.1*	1720	−9.	*	−6.	PKS	c04a
G028.199−0.048	...	5.7	1665		−0.1*		VLA-A	fram03
...	18403−0417	5.7	6035		7.5		Eff	bdwc97
G028.201−0.049	...	5.7	6035		9. *		PKS	c03
G030.60−0.06	OH 30.60	5.5*	1665		0.5		PKS	ch83b
...	...	5.5*	1667		0.5*		PKS	ch83b
G031.412+0.307	...	6.2	1667		−1.0*		VLA-A	fram03
...	G31.4+0.3	6.2	1667		3.0		VLA-C	gm87
G032.744−0.076	...	2.3	1665	−4.2	−3.1*	5.8	VLA-A	fram03
...	...	2.3	6035		−3.3		PKS	cv95
...	...	2.1*	6035		−3.3		PKS	c03
G034.258+0.153	...	3.6*	6035		−4.3*		PKS	c03
G034.257+0.154	G34.3+0.2	3.8	1665	−7.7	−0.7	5.5	VLBA	fraz05
...	...	3.8	1667	−4.1	−1.1*	1.5	VLBA	fraz05
...	...	3.8	1665	−7.8	2.4	8.6	VLBA	zrm00
...	...	3.8	1667	−4.0	−0.5	0.5	VLBA	zrm00
...	...	3.8	1665	−7.7	−5.0	−3.9	MERLIN	gch02
...	...	3.8	1667	−4.1		−4.1	MERLIN	gch02
...	...	3.8	1665	−4.		6.	VLA-CD	grm85
...	...	3.8	1665		0.1		VLA-A	fram03

Table 1. continued.

Source (GL+GB)	Alias name	Dist (kpc)	Freq (MHz)	B_l (mG)	B_m (mG)	B_u (mG)	Obs. telescope	Ref.
...	...	3.8	1667	−0.9		−0.4	VLA-A	fram03
...	...	3.8	1667		−3.0		VLA-C	gm87
...	...	3.8	6035		−4.3		PKS	cv95
...	18507+0110	3.8	6035		−6.2		Eff	bdwc97
G035.025+0.350	...	2.6*	6035		5.0*		PKS	c03
...	...	2.6	6035		5.0		PKS	cv95
G035.024+0.350	...	3.1	1665		2.7*		VLA-A	fram03
...	18515+0157	3.1	6035		5.2		Eff	bdwc97
G035.197−0.743	...	2.2?	1665		3.9		VLA-A	fram03
...	G35.2−0.74N	2.0	1665	−2.5	3.0*	5.2	MERLIN	hc99
G035.577−0.029	...	10.5	1665	−4.8	−4.0*	−6.3	VLBA	fraz05
...	...	10.5	1665	−3.2		−1.2	VLA-A	fram03
G040.426+0.700	...	0.9*	6035		−3.3*		PKS	c03
G040.622−0.137	...	2.1	1665		−5.9*		VLBA	fraz05
...	...	2.1	1667		−6.2		VLBA	fraz05
...	...	2.1	1665	0.1		1.4	VLA-A	fram03
...	...	2.1	1667	−8.7		−1.9	VLA-A	fram03
...	...	2.1	6035		1.7		PKS	cv95
G040.623−0.138	...	2.1*	6035		1.7*		PKS	c03
G042.42+0.70	...	0.8	6035		−3.3*		PKS	cv95
G042.821+0.498	W49N	11.4	1612		−9.1		VLA-C	gm87
...	...	11.4	1665	−7.5	−5.6*	−3.7	VLA-C	gm87
...	...	11.4	1667	−3.1		−3.1	VLA-C	gm87
G043.149+0.013	...	11.4	6035		−4.3*		PKS	c03
G043.165−0.028	W49 S	11.4	1665	0.8	1.5*	5.8	VLA-A	fram03
...	...	11.4	1720	−3.		3.	PKS	c04a
G043.17+0.00	19078+0901	11.4	6035	−5.3	*	−5.0	Eff	bdwc97
G043.795−0.127	...	2.2	6035		3.6*		PKS	c03
G043.796−0.127	...	9.0	1665	−2.6	1.3*	4.5	VLBA	fraz05
...	...	9.0	1667		3.1		VLBA	fraz05
...	...	9.0	6035		3.6		PKS	cv95
...	...	9.0?	1665		0.1		VLA-A	fram03
G045.071+0.134	...	4.7	1665		2.7*		VLA-A	fram03
...	...	4.7	1667		3.6		VLA-A	fram03
...	OH 45.07	4.7	1665	1.8		3.6	MERLIN	bc85
G045.122+0.133	...	6.0	1667		−2.3*		VLA-A	fram03
...	...	6.0	6035		−2.5		PKS	cv95
...	...	6.0	6035		−2.5		PKS	c03
...	OH 45.12	6.0	1665	−2.7		−3.1	MERLIN	bc85
G045.465+0.047	...	5.8	1665		3.7*		VLA-A	fram03
G045.46+0.06	19120+1103	6.0	6035	−5.0	−4.8*	−3.2	Eff	bdwc97
G045.47+0.05	...	7.3?	6035	−5.	*	7.	PKS	cv95
G049.469−0.370	W51	7.3	1720		3.3		VLA-A	fram03
...	...	7.3	1665		6.5*		VLA-C	gm87
...	...	7.3	1720		10.0		VLA-C	gm87
G049.488−0.387	W51e1	7.0	1665	−6.9	−0.6	6.0	VLBA	fraz05
...	W51e1	7.0	1665	6.0		6.0	VLA-CD	grm85
...	W51e1	7.0	1667	−7.0	−2.0	6.0	VLBA	fraz05
...	W51e1	7.0	1720		8.0		VLA-C	gm87
...	W51e2	7.0	1665	4.0	5.6	21.0	VLBA	fraz05
...	W51e2	7.0	1667	3.3	4.3	9.7	VLBA	fraz05
...	W51e2	7.0	1665	5.6		7.5	VLA-C	gm87
...	...	7.0	1667		6.3		VLA-C	gm87
...	...	7.0	1720	10.0		10.0	VLA-C	gm87
...	W51 M/S	7.0	1665		−1.4		VLA-A	fram03
...	W51 M/S	7.0	1720	3.0	3.5*	5.0	VLA-A	fram03
...	W51	7.0	1720	5.0		10.3	VLBI	bmg84
G049.488−0.388	...	6.5	1720		8.8*		PKS	c04a
G049.489−0.388	...	6.5	6035		6.*		PKS	c03

Table 1. continued.

Source (GL+GB)	Alias name	Dist (kpc)	Freq (MHz)	B_l (mG)	B_m (mG)	B_u (mG)	Obs. telescope	Ref.
G049.490−0.387	...	6.5	1720	5.6		10.0	PKS	c04a
...	...	6.5	1665	−1.1		−1.7	VLA-A	fram03
...	...	6.5	1720	3.0		4.0	VLA-A	fram03
...	...	6.5	6035		4.7		PKS	cv95
...	W51	6.5	6035		3.6*		EVN+	db98
...	19213+1424	6.5	6035		3.9		Eff	bdwc97
G049.490−0.388	...	6.5	6035		5.*		PKS	c03
G069.540−0.976	ON 1	3.0	1665	−5.1	−4.4	−1.2	VLBA	fraz05
...	ON 1	3.0	1667		−0.9		VLBA	fraz05
...	...	3.0	1665	−3.6	−0.2	−0.2	VLA-A	fram03
...	...	3.0?	6031		−6.3		EVN+	db98
...	...	3.0?	6035	−5.3	−3.6*	−3.6	EVN+	db98
...	20081+3122	3.0?	6035	−2.7		−4.8	Eff	bdwc97
...	...	3.0?	6031		−4.2		Eff	bdwc97
...	...	3.0?	13 441	−8.3		−3.8	GBT	frm05
G070.293+1.601	K3-50	8.7?	1665	−7.5	−2.7	−2.6	VLBA	fraz05
...	...	8.7	1667		−2.6*		VLBA	fraz05
...	...	8.7	1665		−2.5		VLA-A	fram03
...	...	8.7	1667		−2.6		VLA-A	fram03
...	19598+3324	8.7	6035	−5.3		−9.1	Eff	bdwc97
G075.782+0.343	ON 2 N	5.6	1665	3.0	4.6	5.6	VLBA	fraz05
...	ON 2 N	5.6	1667	1.6	2.6*	5.0	VLBA	fraz05
G078.887+0.709	AFGL 2591	1.0	1665	0.5	0.6*	3.8	MERLIN	hc05
...	...	1.0	1667		−1.6		MERLIN	hc05
G080.87+0.42	20350+4126	4.8	6035		−4.3		Eff	bdwc97
...	DR20	4.8	6031		−2.7*		Eff	bdwc97
G081.721+0.571	W75 S	2.0	1665	−7.6	−3.8*	6.6	VLBA	fraz05
...	...	2.0	1665	−4.6		6.1	VLA-A	fram03
...	W75S(3)	2.0	6035		−3.0		Eff	bdwc97
G081.871+0.781	W75 N	2.0	1665	−7.4	4.3	8.1	VLBA	fraz05
...	...	2.0	1667	−6.9	−4.2	7.6	VLBA	fraz05
...	...	2.0	1665	0.1		5.3	VLA-A	fram03
...	...	2.0	1667	−0.2		9.4	VLA-A	fram03
...	...	2.0	6035	7.5		7.8	Eff	bdwc97
...	...	2.0	1665	5.2		7.7	VLBA	smv+02
...	...	2.0	1665	1.0	2.4*	8.1	MERLIN	bcd+86
G106.80+5.31	22176+6303	1.4	6035		2.8*		Eff	bdwc97
G109.871+2.114	Cep A	0.7	1665	−5.5	3.2*	10.4	VLBA	fraz05
...	...	0.7	1667	−6.4	−5.5	3.2	VLBA	fraz05
...	...	0.7	1665	−4.4	3.7	12.7	MERLIN	bscr05
...	...	0.7	1667	−6.5		3.1	MERLIN	bscr05
...	...	0.7	1720		17.3		MERLIN	bscr05
...	...	0.7	1720		17.3		MERLIN	nscr04
...	...	0.7	1665	−3.5		3.4	VLA-A	fram03
...	...	0.7	1667		3.2		VLA-A	fram03
...	22543+6145	0.7	6035		4.8		Eff	bdwc97
G111.543+0.777	NGC 7538	2.8	1665		0.7		VLBA	fraz05
...	... IRS 1	2.8	1667		2.0		MERLIN	hc03
...	... IRS 1	2.8	1720		1.7*		MERLIN	hc03
G111.533+0.757	NGC 7538	2.8	1665		2.3		VLA-A	fram03
G133.946+1.064	W3 OH	2.2	1612		5.2		VLA-A	fram03
...	...	2.2	1667	−0.2		6.4	VLA-A	fram03
...	...	2.2	1612	4.7	7.6	10.7	VLBA	wgd04b
...	...	2.2	1665	3.1	5.6	12.8	VLBA	wgd04a
...	...	2.2	1667	2.4	6.6	7.0	VLBA	wgd04b
...	...	2.2	1720	4.5	6.0*	7.5	VLBA	wgd04b
...	...	2.2	1720		5.3		VLA-A	fram03
...	W3(OH)	2.2	6031	5.7	8.9	14.6	EVN+	dbw+98
...	...	2.2	6035	0.9	4.4	9.7	EVN+	dbw+98

Table 1. continued.

Source (GL+GB)	Alias name	Dist (kpc)	Freq (MHz)	B_l (mG)	B_m (mG)	B_u (mG)	Obs. telescope	Ref.
...	W3(OH)	2.2	13 441	5.6	10.2	11.3	VLBA	bd98
...	W3 OH	2.2	6035	7.1	8.0	8.7	Eff	bdwc97
...	...	2.2	6031	3.3	4.7	8.1	Eff	bdwc97
...	...	2.2	13 441	6.9	8.2	11.3	GBT	frm05
...	...	2.2	13 434		10.3		GBT	frm05
G196.454−1.677	S269	3.8	1665	−4.2	*	−4.0	VLBA	fraz05
...	...	3.8	1665		−4.5		VLBA	fraz05
G208.994−19.38	Orion	0.5	1665		*	−2.5	VLBI	hmr+77
G213.706−12.606	Mon R2	0.9	1665	−2.6	−2.4*	−2.2	VLBA	fraz05
...	...	0.9	1667	−2.5	−2.5	−2.2	VLBA	fraz05
...	...	0.9	1665		−3.4		VLA-A	fram03
G285.263−0.050	...	4.3	6035		10.0		PKS	cv95
...	...	4.3	6035		10.0*		PKS	c03
G290.375+1.666	...	3.0	1720		7.5*		PKS	c04a
G294.511−1.621	...	1.7	6035		1.1		PKS	cv95
...	...	1.7	6035		1.1*		PKS	c03
G300.969+1.148	...	4.3	6035		−4.0		PKS	cv95
...	...	4.3	6030		−5.0		PKS	c03
...	...	4.3	6035		−5.0*		PKS	c03
...	OH 300.97	4.3	1665		−1.3		PKS	ch87
...	...	4.3	1720		−5.5		PKS	c04a
G305.81−0.24	...	3.2*	1665		−2.7*		PKS	ch87
G306.322−0.334	...	1.4	1720		6.0*		PKS	c04a
G309.921+0.479	...	5.4	6035	−2.5	*	3.5	PKS	cv95
...	...	5.4	13 441	−3.6	0.0	3.3	PKS	c04b
G310.146+0.760	...	3.4	1720	−16.	*	5.	PKS	c04a
G311.596−0.398	...	13.9	6035		3.5*		PKS	cv95
...	...	13.9	13 441		5.4		PKS	c04b
G323.459−0.079	OH 323.459	4.1	1665	1.5	2.5	4.1	LBA	cr01
...	...	4.1	1667			2.5	LBA	cr01
...	...	4.1*	6035		2.5		PKS	cv95
...	...	4.1	6035		3.5		PKS	cr01
...	...	4.1	6035		2.5*		PKS	c03
G328.808+0.633	...	2.6	6035		−4.*		PKS	c03
G328.809+0.633	...	2.6*	1720		1.5		PKS	c04a
...	...	2.6*	13 441		3.6*		PKS	c04b
...	...	2.6	6035		3.7		PKS	c03
G329.066−0.308	...	2.6	6035		−1.7*		PKS	c03
G329.339+0.148	...	7.3	1720		4.		PKS	c04a
...	...	7.3	6035		13.		PKS	c03
...	...	7.3	13 441		10.7*		PKS	c04b
G329.405−0.459	...	4.3*	6035		3.5		PKS	cv95
...	...	4.3*	6035		3.5*		PKS	c03
G329.426−0.158	...	4.8	1720		−2. *		PKS	c04a
G330.953−0.182	...	5.7*	6035		−2.5		PKS	cv95
...	...	5.7*	1720		2.		PKS	c04a
...	...	5.7*	6035		−2.5*		PKS	c03
G330.96−0.18	...	5.7*	1665		−4.5*		PKS	chg80
...	...	5.7*	1667		−4.5		PKS	chg80
G330.34−0.34	...	4.7	1665		2. *		PKS	chg80
G331.542−0.066	...	5.8	6030		1.8		PKS	c03
...	...	5.8	6035		1.8*		PKS	c03
...	...	5.8	13 441	−3.0	2.4	3.1	PKS	c04b
G332.826−0.549	...	3.2*	6035		2.*		PKS	c03
G333.135−0.431	...	3.2	6035		−3.3*		PKS	c03

Table 1. continued.

Source (GL+GB)	Alias name	Dist (kpc)	Freq (MHz)	B_l (mG)	B_m (mG)	B_u (mG)	Obs. telescope	Ref.
...	...	3.2	6035		−3.3		PKS	cv95
G333.36−0.14	...	5.4*	6035		−4.0*		PKS	cv95
G333.608−0.215	...	3.2	6035		−1.5*		PKS	c03
...	...	3.2	6035		−1.5		PKS	cv95
G336.358−0.137	...	5.4*	6035		−4.0*		PKS	c03
G336.822+0.028	...	5.4*	6035		−5.0		PKS	cv95
...	...	5.4*	1720		−6*		PKS	c04a
G336.822+0.028	...	5.4*	6035		−5.0*		PKS	c03
G336.941−0.156	...	4.4*	1720		6. *		PKS	c04a
...	...	4.4*	13441		7.4		PKS	c04b
G336.994−0.027	...	7.8	1720		−3.*		PKS	c04a
G337.404−0.402	...	3.1*	6035		3.7*		PKS	c03
G337.613−0.060	...	3.0*	1720		−5.7		PKS	c04a
...	...	3.0*	6035		−4.3		PKS	cv95
...	...	3.0	6035		−4.3*		PKS	c03
G337.705−0.053	...	12.1	6035		−4.0		PKS	cv95
...	...	12.1	1665		−4.0*		PKS	c03
...	...	12.1	1667		−4.0		PKS	c03
G337.71−0.06	...	12.1	1665		−2.0*		PKS	chg80
...	...	12.1	1667		−2.0		PKS	chg80
G337.92−0.48	...	3.1	1665		−3.0*		PKS	chg80
...	...	3.1	1667		−3.0		PKS	chg80
G339.622−0.121	...	2.8*	6035		−1.6*		PKS	c03
G339.884−1.259	...	2.6	1720		−6.0		PKS	c04a
...	...	2.6	6035		−3.6*		PKS	c03
G339.62 −0.12	...	2.8*	6035		−1.6*		PKS	cv95
G340.785−0.096	...	8.0	1720	−8.		−5.	PKS	c04a
...	...	8.0	6035	−6.	*	2.5	PKS	c03
G341.219−0.212	...	3.2	1665		5.8*		VLA-A	fram03
...	OH 341.21	3.2	1665		6.		PKS	ch83a
G343.128−0.063	...	3.1	1665		3.7*		VLA-A	fram03
G344.419+0.044	...	2.9*	6035		−5.8*		PKS	c03
...	...	2.9	6035		−5.8		PKS	cv95
G344.581−0.022	...	0.6	1665	−2.8	*	5.5	VLA-A	fram03
G345.003−0.224	...	2.9	1720		3.5		PKS	c04a
...	...	2.9	1720		6.2		PKS	c04a
...	...	2.9	1720		1.9		VLA-A	fram03
...	G345.0−0.2	2.9	1720		6.4		VLA-C	gm87
...	...	2.9	6035		4.0		PKS	cv95
...	...	2.9	6035		4.0*		PKS	c03
...	...	2.9	13 441	2.9		5.1	PKS	c04b
G345.011+1.792	...	2.2	1665	−2.5	*	4.2	VLA-A	fram03
G345.118+1.592	...	1.8	1720		−1.5*		PKS	c04a
G345.487+0.314	...	1.8*	6035		2.*		PKS	c03
G345.495+1.462	...	2.5	1720		12.*		PKS	c04a
G345.497+1.462	...	2.1	1720		10.*		PKS	c04a
G345.50 +0.35	...	1.8*	6035		2.0*		PKS	cv95
G345.505+0.347	...	2.1	1665		−1.6		VLA-A	fram03
...	...	2.1	1667	0.1	*	0.9	VLA-A	fram03
G345.699−0.090	...	1.6	1665		0.4*		VLA-A	fram03
G347.628+0.149	...	10.4	1612		3.1*		VLA-A	fram03
...	...	10.4	6035		3.8		PKS	c03
...	...	10.4*	6035		−4.2		PKS	cv95
G348.549−0.978	...	2.2	1665		5.8		VLA-A	fram03
...	...	2.2	1720		−2.6*		VLA-A	fram03
G348.550−0.979	...	1.8*	1720		−5.		PKS	c04a
...	...	1.8	1720		−6.4		VLA-C	gm87
...	G348.5−1.0	1.8	1665		−1.9		VLA-C	gm87
...	...	1.8	1667		−3.1*		VLA-C	gm87
...	...	1.8*	6035		−3.3		PKS	cv95
...	...	1.8	6035		−3.3		PKS	c03
G350.011−1.341	...	3.1	1665		0.7*		VLA-A	fram03
G350.113+0.095	...	8.3	6035		−3.3*		PKS	c03
...	...	8.3*	6035		−3.3		PKS	cv95

Table 1. continued.

Source (GL+GB)	Alias name	Dist (kpc)	Freq (MHz)	B_l (mG)	B_m (mG)	B_u (mG)	Obs. telescope	Ref.
G350.686−0.491	...	2.3*	1720	−3.5		−4.9	PKS	c04a
...	...	2.3*	6035	−1.	*	−2.7	PKS	c03
G351.161+0.697	NGC 6334B	2.3	1667	0.1	*	0.2	VLA-A	fram03
G351.416+0.646	NGC 6334F	2.0	1665		−5.3*		VLA-A	fram03
...	...	2.0	1667		−4.2		VLA-A	fram03
...	...	2.0	1720		−3.1		VLA-A	fram03
...	...	2.0	1665		−5.6		VLA-C	gm87
...	...	2.0	1720		−6.2		VLA-C	gm87
G351.417+0.645	NGC 6334F	2.0	1720		−6.4		PKS	c04a
...	OH 351.41	2.0	1665		−5.7		PKS	ch83a
...	...	2.0	6035		−4.0		PKS	cv95
...	...	2.0	6030		−4.8		PKS	c03
...	...	2.0	6035		−4.8		PKS	c03
G351.581−0.353	...	6.7	6035		2.0*		PKS	c03
...	...	6.7	6035		2.0		PKS	cv95
G351.582−0.352	...	6.7	1665		−4.9*		VLA-A	fram03
G351.775−0.536	...	1.9	1720	−6.		3.	PKS	c04a
...	...	1.9	6035		−3.3*		PKS	c03
...	...	1.9	6035		−3.3		PKS	cv95
...	...	1.9	1665		−3.3		PKS	c04a
G351.775−0.538	...	2.2	1665	−5.9	−3.6	5.4	VLBA	fraz05
...	...	2.2	1667	−3.7	4.0	5.5	VLBA	fraz05
...	...	2.2	1665	−6.1	0.2*	0.3	VLA-A	fram03
...	...	2.2	1667	−3.7	−0.8	5.7	VLA-A	fram03
G353.410−0.360	...	3.8	1720		−2.3*		PKS	c04a
...	OH 353.41	3.8	1665		−1.9		PKS	ch83a
...	...	3.8	6030		−9.1		ATCA	c01
...	...	3.8	6035		−1.1		PKS	cv95
...	...	3.8	6035		−8.9		ATCA	c01
...	...	3.8	6035	−9.0	−1.1		PKS	c03
G353.410−0.361	...	3.8	1665		1.2*		VLA-A	fram03
G354.724−0.300	...	8.5	6035		4.3*		PKS	c03
...	...	8.5	1665		6.8		PKS	c98
G354.73 +0.29	...	8.5	6035		4.3*		PKS	cv95
G355.345+0.146	...	23.	1665		−4.4*		VLA-A	fram03
G355.344+0.147	...	1.7	6035		−4.3*		PKS	c03
...	...	1.7*	6035		−4.3		PKS	cv95
...	OH 355.34	1.7	1665		−4.5		PKS	ch83a
G359.138+0.032	...	3.1	1665	−4.7	*	0.2	VLA-A	fram03
G359.436−0.103	...	8.2	1665		−0.5*		VLA-A	fram03
G359.956−0.042	SgrA	8.5	1720	−2.8	*	−4.8	VLA-A	yrg+99
G359.934−0.065	SgrA	8.5	1720	1.8	*	3.7	VLA-A	yrg+99

Notes:
1. B_l & B_u are the two extrema of magnetic field strengths of many maser spots in high resolution VLBI observations; we also give magnetic fields in B_m if there is only measurement for one spot. In low resolution single dish observations we give magnetic field strength in B_m, but if there are many B-values for different velocities, then we give two extrama for B_l and B_u as well as B_m. Signs are values extracted from the paper are markes with "*".
2. Distance: in kpc, (with 8.5/220 frame). If there is an ambiguity in kinematic distances, we take the nearer one and marked with "*".
3. Positive B value indicates the field pointing away from us, and negative towards us.

References for Table 1:

bc85: Baart & Cohen 1985, MNRAS, 213, 641;
bcd+86: Baart et al. 1986, MNRAS, 219, 145;
bfgt00: Brogan et al. 2000, ApJ, 537, 875;
bgyr03: Bains et al. 2003, MNRAS, 338, 287;
brgy04: Bains et al. 2004, MNRAS, 354, 529;
bscr05: Bartkiewicz et al. 2005, MNRAS, 361, 623;
bd98: Baudry & Diamond 1998, A&A, 331, 697;
bdwc97: Baudry et al. 1997, A&A, 325, 255;
bmg84: Benson et al. 1984, AJ, 89, 1391;
c98: Caswell 1998, MNRAS, 297, 215;
c01: Caswell 2001, MNRAS, 326, 805;
c03: Caswell 2003, MNRAS, 341, 551;
c04a: Caswell 2004a, MNRAS, 349, 99;
c04b: Caswell 2004b, MNRAS, 352, 101;
ch83a: Caswell & Haynes 1983a, Aust. J. Phys., 36, 361;
ch83b: Caswell & Haynes 1983b, Aust. J. Phys., 36, 417;
ch87: Caswell & Haynes 1987, Aust. J. Phys., 40, 215;
chg80: Caswell et al. 1980, Aust. J. Phys., 33, 639;
cv95: Caswell & Vaile 1995, MNRAS, 273, 328;
cr01: Caswell & Reynolds 2001, MNRAS, 325, 1346;
db98: Desmurs & Baudry 1998, A&A, 340, 521;
dbw+98: Desmurs et al. 1998, A&A, 334, 1085;
efce05: Edris et al. 2005, A&A, 434, 213;
fram03: Fish et al. 2003, ApJ, 596, 328;
fraz05: Fish et al. 2005a, ApJS, 160, 220;
frm05: Fish et al. 2005b, ApJ, 623, 269;
gch02: Gasiprong et al. 2002, MNRAS, 336, 47;
grm85: Garay et al. 1985, ApJ, 289, 681;
gm87: Gaume & Mutel 1987, ApJS, 65, 193;
hmr+77: Hansen et al. 1977, ApJ, 218, L65
hc99: Hutawarakorn & Cohen, 1999, MNRAS, 303, 845;
hc03: Hutawarakorn & Cohen, 2003, MNRAS, 345, 175;
hc05: Hutawarakorn & Cohen, 2005, MNRAS, 357, 338;
hcb02 Hutawarakorn et al. 2002, MNRAS, 330, 349;
nscr04: Niezurawska et al. 2004, MNRAS, 350, 1409;
sgc+06: Stark et al. 2006, ApJ, in press ([astro-ph/0610137]);
str01: Sarma et al. 2001, ApJ, 554, L217;
smv+02: Slysh et at 2002, ApJ, 564, 317;
sg04: Szymczak & Gerard 2004, A&A, 423, 209;
scr02: Szymczak et al. 2001, A&A, 371, 1012;
wgd04a: Wright et al. 2004a, MNRAS, 350, 1253;
wgd04b: Wright et al. 2004b, MNRAS, 350, 1272;
yrg+99: Yusef-Zadeh et al. 1999, ApJ, 512, 230;
zrm00: Zheng et al. 2000, A&A, 357, L37.

References for Table 2:

bmrh01: Bourke et al. 2001, ApJ, 554, 916;
bt01a: Brogan & Troland 2001a, ApJ, 550, 799;
bt01b: Brogan & Troland 2001b, ApJ, 560, 821;
bta+05: Brogan et al. 2005, ASP Conf. Ser., 343, 183;
btrc99: Brogan et al. 1999, ApJ, 515, 304;
c99: Crutcher 1999, ApJ, 520, 706;
ck83: Crutcher & Kazés 1983, A&A, 125, L23;
ckt87: Crutcher et al. 1987, A&A, 181, 119;
crmt96: Crutcher et al. 1996, ApJ, 462, L79;
crtg99: Crutcher et al. 1999a, ApJ, 515, 275;
ct00: Crutcher & Troland, 2000, ApJ, 537, L139;
ctg+93: Crutcher et al. 1993, ApJ, 407, 175;
ctl+99: Crutcher et al. 1999b, ApJ, 514, L121;
frm05: Fish et al. 2005b, ApJ, 623, 269;
gh94: Goodman & Heiles 1994, ApJ, 424, 208;
gch+89: Goodman et al. 1989, ApJ, 338, L61;
kc86: Kazés & Crutcher 1986, A&A, 164, 328;
ktch88: Kazés et al. 1988, ApJ, 335, 263;
mggh95: Myers et al. 1995, ApJ, 442, 177;
strc00: Sarma et al. 2000, ApJ, 533, 271;
rctg93: Roberts et al. 1993, ApJ, 412, 675;
rct95: Roberts et al. 1995, ApJ, 442, 208;
tck86: Troland et al. 1986, ApJ, 304, L57;
tcgh89: Troland et al. 1989, ApJ, 347, L89;
tcg+96: Troland et al. 1996, ApJ, 471, 302;
vg90: van der Werf & Goss, 1990, A&A, 238, 296;
vgh+93: van der Werf et al. 1993, ApJ, 411, 247.

Table 2. Magnetic field measurements from Zeeman splitting of molecular clouds.

Source (GL+GB)	Alias name	Dist (kpc)	B (μG)	σ_B (μG)	abs./emi. line	Freq. (MHz)	Obs. telescope	Ref.	Remarks
G000.70−00.04	SgrB2 NSW-Z	8.20	−720	160	absp-HI	1420	VLA-BA	crmt96	
...	SgrB2 Main-Z	8.20	−480*	110	absp-HI	1420	VLA-BA	crmt96	B-variable
G014.00−00.60	G14.0−0.6	2.4	+64*	18	absp-OH	1665/7	GB43	bmrh01	
G015.00−00.70	M17SW (core)	2.2	−450	100	absp-HI	1420	VLA-DC	btrc99	GMC-complex
...	M17NW	2.2	+550	100	absp-HI	1420	VLA-DC	btrc99	B-structure
G015.00−00.70	M17SW	2.2	+150*	50	absp-OH	1665	VLA-CB	bt01b	GMC-complex
...	M17SW	2.2	+260	45	absp-HI	1420	VLA-CB	bt01b	B-structure
G028.80+03.48	W40	0.37	−14*	3	absp-OH	1665/7	Nancay	ckt87	HII-MC
G043.3−00.2	W49B	8.0	+21*	5	absp-OH	1665/7	Nancay	ckt87	DarkCloud#SNR
G043.17−00.01	W49A $v = 4$	11.4	−145*	20	absp-HI	1420	VLA-B	bt01a	SFR-HII
G043.17−00.00	W49A $v = 7$	11.4	+270	20	absp-HI	1420	VLA-B	bt01a	SFR-HII
G061.50+00.10	S88B	2.2	+69	5	absp-OH	1665/7	Nancay	ckt87	HII knot
...	...	2.2	+47	3	emis-OH	1665/7	Arcb	gch+89	MC-core
...	...	2.2	+49*	2	absp-OH	1665	Arcb	ct00	Cal-obs
G076.40−00.62	S106	0.60	+137*	17	absp-OH	1665/7	GB43	ktch88	bipolarN
G076.38−00.62	S106(IRS4)	0.60	+400	23	absp-OH	1665/7	VLA-C	rct95	bi-P HII
...	S106(inner)	0.60	+300	100	absp-OH	1665/7	VLA-C	rct95	bi-P HII
G076.38−00.62	S106(center)	0.60	+70	12	absp-HI	1420	VLA-C	rct95	bi-P HII
G081.70+00.57	DR21OH1	3.0	−360*	100	emis-CN	113 000	IRAM30	ctl+99	
...	DR21OH2	3.0	−710	120	emis-CN	113 000	IRAM30	ctl+99	
G133.70+01.18	W3(main)	2.2	+73	7	absp-OH	1665/7	Nancay	kc86	
G133.70+01.20	W3 core	2.2	−120	20	absp-HI	1420	VLA-D	tcgh89	B-map
G133.71+01.23	W3 core	2.2	+80	20	absp-HI	1420	VLA-D	tcgh89	reversed B
G133.72+01.22	W3A	2.2	+16	6	absp-HI	1420	WSRT	vg90	B-structure
G133.71+01.21	W3B	2.2	+37	16	absp-HI	1420	WSRT	vg90	B-structure
G133.69+01.22	W3cd	2.2	−76	25	absp-HI	1420	WSRT	vg90	B-structure
G133.72+01.22	W3A $V = -46$	2.2	+18	3	absp-HI	1420	VLA-C	rctg93	hourglass B
G133.72+01.22	W3A $V = -38$	2.2	−47	3	absp-HI	1420	VLA-C	rctg93	hourglass B
G133.71+01.21	W3B $V = -38$	2.2	+103	7	absp-HI	1420	VLA-C	rctg93	hourglass B
G133.71+01.21	W3B $V = -46$	2.2	+15	4	absp-HI	1420	VLA-C	rctg93	hourglass B
G133.69+01.22	W3cd $V = -38$	2.2	+36*	6	absp-HI	1420	VLA-C	rctg93	hourglass B
G133.74+01.18	W3K $V = -38$	2.2	+33	8	absp-HI	1420	VLA-C	rctg93	hourglass B
G133.74+01.18	W3K $V = -46$	2.2	+39	7	absp-HI	1420	VLA-C	rctg93	hourglass B
G133.73+01.15	W3-NGC896-1 v1	2.2	+43	7	absp-HI	1420	VLA-C	rctg93	hourglass B
G133.73+01.15	W3-NGC896-1 v2	2.2	+18	6	absp-HI	1420	VLA-C	rctg93	hourglass B
G133.71+01.12	W3-NGC896-2-3	2.2	−38	5	absp-HI	1420	VLA-C	rctg93	hourglass B
G133.71+01.12	W3-NGC896-2	2.2	+19	5	absp-HI	1420	VLA-C	rctg93	hourglass B
G133.71+01.12	W3-NGC896-3	2.2	−40	7	absp-HI	1420	VLA-C	rctg93	hourglass B
G134.00+01.06	W3OH	2.2	+3000	300	absp-OH	13 434	GBT	frm05	
G159.20−20.12	B1	0.35	−19*	4	emis-OH	1665/7	GB43	ctg+93	dark cloud
...	...	0.35	−27	4	emis-OH	1665/7	Arcb	gch+89	dark cloud
G178.00−09.73	L1544 core	0.14	+11*	2	emis-OH	1665/7	Arcb	ct00	dark cloud
G209.0−19.4	Orion A	0.41	−125	20	absp-OH	1665/7	Nancay	tck86	data overlook?
G209.0−19.4	Orion A	0.41	−49*	4	absp-HI	1420	Nancay	tck86	data overlook?
G209.0−19.4	Orion A Trapez	0.41	−50	8	absp-HI	1420	VLA	bta+05	
G209.0−19.4	Orion A DarkBay	0.41	−300	25?	absp-HI	1420	VLA	bta+05	
G208.99−19.39	Orion B	0.415	+38*	1	absp-OH	1665/7	Nancay	ck83,kc86	
G206.54−16.37	NGC 2024(OrionB)	0.415	+87	6	absp-OH	1665/7	VLA-D	crtg99	B-peak.Vary
...	W12	0.415	+52	9	absp-HI	1420	VLA-D	crtg99	B-peak.Map
...	Orion B v1	0.415	+28	8	absp-HI	1420	VLA-D	vgh+93	B-peak.Map
...	Orion B v2	0.415	+63	8	absp-HI	1420	VLA-D	vgh+93	B-peak.Map
...	...	0.415	+35*	2	absp-OH	1665/7	PKS	bmrh01	cal-obs
...	...	0.415	+34	3	absp-OH	1665/7	GB43	bmrh01	cal-obs
G208.99−19.38	OCM-1n	0.45	−360*	80	emis-CN	113 000	IRAM30	ctl+99	
G267.90−01.09	RCW38	0.7	+38*	3	absp-OH	1665/7	PKS	bmrh01	Bright-HII
G291.30−00.70	RCW 57	3.1	−203	24	absp-OH	1665/7	PKS	bmrh01	HII region
...	...	3.1	−13*	4	absp-OH	1665/7	PKS	bmrh01	
G327.30−00.55	G327.3−0.5	3.3	−13*	4	absp-OH	1665/7	PKS	bmrh01	
G351.34+00.75	NGC 6334	1.7	+15	4	absp-OH	1665/7	PKS	bmrh01	
G351.25+00.66	NGC 6334A	1.7	+153	16	absp-OH	1665/7	VLA-CB	strc00	GMC-complex
G351.37+00.65	NGC 6334D	1.7	−93*	13	absp-HI	1420	VLA-CB	strc00	GMC-complex
G351.43+00.66	NGC 6334E	1.7	−175	28	absp-HI	1420	VLA-CB	strc00	GMC-complex
G353.10+16.66	rho-Oph1	0.13	+10*	3	emis-OH	1665/7	GB43	tcg+96	dark cloud
G353.1+00.7	W22A	0.15	−18*	1	absp-OH	1665/7	Nancay	kc86	HII-complex
G353.20+00.89	W22B	0.15	−32*	9	absp-OH	1665/7	Nancay	ckt87	HII-complex